Nuclear Fragmentation/Dispersion Modeling and Simulation of Hazardous Near-Earth Objects

2011 IAA Planetary Defense Conference

09-12 May 2011

Bucharest, Romania

Brian Kaplinger[(1)], Bong Wie[(1)], David Dearborn[(2)]

[(1)]Asteroid Deflection Research Center
Iowa State University
2271 Howe Hall, Room 1200
Ames, IA, 50011, United States
Email: bongwie@iastate.edu

[(2)]Lawrence Livermore National Laboratory
7000 East Avenue
Livermore, CA, 94550, United States
Email: dearborn2@llnl.gov

INTRODUCTION

A major bottleneck in determining appropriate mitigation methods for Near-Earth Objects (NEOs) has been a lack of experimental data on the efficacy of each approach, forcing a reliance on simulations to determine mission effectiveness. As we move from the concept stage into true mission planning for effective NEO threat mitigation, we must depart from simulation of a few sample cases and instead use actual mission parameters to integrate modeling and simulation into the mission design cycle. This paper presents the development of simulation tools designed to be implemented as part of the mission design procedure for nuclear fragmentation and dispersion of an NEO. A description of the methods used will be presented, followed by a discussion of the advanced GPU (Graphics Processing Unit) computing technology applied to accelerate computation. Preliminary results of a fragmented NEO dispersion scenario are discussed, emphasizing global parameter search methods for use in engineering mission analysis. A model of the NEO fragmentation process is presented for a subsurface nuclear explosion and penetrating contact burst. A Smoothed Particle Hydrodynamics (SPH) code is used to compare the results to past studies of nuclear shock propagation in brittle material and current research in hypervelocity impacts. This approach is contrasted to Arbitrary Lagrangian-Eulerian (ALE) codes in current use at the Lawrence Livermore National Laboratory for asteroid fragmentation simulation.

We assume an isotropic Weibull distribution of implicit flaws in the NEO material and conduct Monte Carlo simulation to establish a mean response of the target NEO to the fragmentation process. Resulting coherent masses are propagated through a model of solar system dynamics until the predetermined date of impact. Masses remaining on impact trajectories undergo a simulation of reentry into Earth's atmosphere, resulting in final tallies of mass missing the Earth, fragments on capture trajectories, airburst events, and impacts of reduced-mass fragments. Past results show that, on some orbits, the impacting mass can be reduced to lower than 0.1% of the NEO mass. The present paper addresses a modular framework for NEO structures to provide guidelines for mission design analysis.

Historically, simulations have been limited to a few large test cases to demonstrate the viability of planetary defense options. This paper addresses the use of GPU computation, a new direction in high-performance computing (HPC), to achieve up to 150x faster computation in a workstation form factor [1]. A dedicated compute server has been shown to be over 400x as fast as CPU implementation, and these are far cheaper than their HPC cluster and supercomputer counterparts [2,3]. This has allowed for a revolution in computing on a budget, allowing hundreds of complex simulations to be tested. While new HPC technology is shown to solve old problems faster, this paper also addresses the identification of new problems that were previously intractable without the use of a supercomputer. Specific performance and results from several GPU compute configurations will be presented. Disruption of an NEO (i.e. fragmentation and dispersion) has been shown to be a viable option using current technology for worst-case mission scenarios with a short warning time. An extended characterization of disruption scenarios is discussed, and an effort is made to determine needed technological requirements for general nuclear disruption effectiveness. Use of improvements to fragmentation modeling, reentry modeling, and orbital dispersion modeling [1] are presented.

FRAGMENTATION MODEL

This section presents the asteroid models being considered. While spherical bodies have been assumed for convenience, it is important to note that any valid three-dimensional geometry can be processed by the current simulation framework. The resulting fragmented system is intended to be statistical in nature, so a Direct Simulation Monte Carlo approach (DSMC) is taken to identify expected system characteristics.

Previous ALE Static Results

In previous work [2,4,5], a 270-m diameter Apophis-like asteroid model was developed with a total mass of 2.058E10 kg. This model was comprised of two main parts (inhomogeneous), as shown in Fig. 1. The core of the asteroid was solid granite with a density of 2630.0 kg/m^3, while the outer mantle was a "rubble pile" of density 1910 kg/m^3. This results in a bulk asteroid density of 1990 kg/m^3, similar to that measured for the asteroid Itokawa. Linear strength modeling was used in the core, with a yield strength of 14.6 MPa and a shear modulus of 35 MPa. A static (non-moving) nuclear explosive is detonated in a 5 meter subsurface cavity, resulting in an energy source equivalent to 300 kilotons [4]. The resulting system shown in Fig. 2 has a clear direction of maximum momentum, with radially distributed fragments dispersing from the center of mass with velocities far in excess of the local escape velocity. The orbital dynamics of this system for an orbit similar to that of Apophis has been extensively studied [1,2,5], and this deflection could result in as little as 0.1% of the asteroid mass remaining on impacting trajectories.

Smoothed Particle Hydrodynamics Model

For the purposes of the present simulation study, a meshless hydrodynamics model was desired. This approach would eliminate the need for storing and updating a grid, simplify calculations for large deformations, and allow for contiguous memory access to local field properties. The SPH formulation [6,7] was chosen to satisfy the first two goals, while the latter will be discussed with regards to the GPU implementation. The core idea of SPH is to approximate a field property $f(x)$ by using a mollifier W (also known as an approximate identity) with compact support:

$$\langle f(x)\rangle = \int_{\Omega} f(s)W(x-s)\,ds, \quad W \in C_0^1\left(\mathbb{R}^n\right), \quad \Omega = \operatorname{supp}(W) \tag{1}$$

where the brackets indicate the SPH approximation [7], allowing the field variables to be computed as a sum over the nearest neighbor particles representing the flow. In the present formulation, W is taken as the cubic spline kernel [6,7], with a variable isotropic domain of support with radius h. Changing h in space and time allows for the simulation to respond to changes in flow conditions with a change in local resolution [6,7]. A mass m is assigned to each particle representative in the model, as well as initial position and velocity components (x^β and v^β) in each β direction. Material properties such as density, ρ, and specific energy, e, complete the state description. Similar to the above integral relationship, derivatives and integrals of field functions can be approximated, resulting in the following set of equations [6-8] involving the kernel derivative (a scalar valued function of vector position $\mathbf{x}$):

$$\begin{aligned}
\frac{Dx_i^\alpha}{Dt} &= v_i^\alpha \\
\frac{D\rho_i}{Dt} &= \sum_{j=1}^{N} m_j\left(v_i^\beta - v_j^\beta\right)\frac{\partial W}{\partial x^\beta}\left(\mathbf{x}_j - \mathbf{x}_i\right) \\
\frac{Dv_i^\alpha}{Dt} &= -\sum_{j=1}^{N} m_j\left(\frac{\sigma_i^{\alpha\beta}}{\rho_i^2} + \frac{\sigma_j^{\alpha\beta}}{\rho_j^2} + \Pi_{ij}\right)\frac{\partial W}{\partial x^\beta}\left(\mathbf{x}_j - \mathbf{x}_i\right) + F_i^\alpha \\
\frac{De_i}{Dt} &= \frac{1}{2}\sum_{j=1}^{N} m_j\left(\frac{P_i}{\rho_i^2} + \frac{P_j}{\rho_j^2} + \Pi_{ij}\right)\left(v_i^\beta - v_j^\beta\right)\frac{\partial W}{\partial x^\beta}\left(\mathbf{x}_j - \mathbf{x}_i\right) + \frac{1}{\rho_i}S_i^{\alpha\beta}\varepsilon_i^{\alpha\beta} + H_i
\end{aligned} \tag{2}$$

where repeated indices in a product indicate implied summation over all possible values, $\sigma^{\alpha\beta}$ is the stress tensor, P is the pressure, $S^{\alpha\beta}$ is the deviatoric (traceless) stress tensor, $\varepsilon^{\alpha\beta}$ is the local strain rate tensor, F represents external forces, and H represents energy sources. Π represents the Monaghan numerical viscosity [7,9] used to resolve shocks, accommodate heating along the shock, and resist unphysical material penetration. The material strength model for the core uses an elastic-perfectly plastic description of strength [6-8], where the hydrodynamic stress is determined as:

$$\sigma_i^{\alpha\beta} = -P_i\delta^{\alpha\beta} + (1-\eta)S_i^{\alpha\beta}, \quad \eta \in [0,1] \tag{3}$$

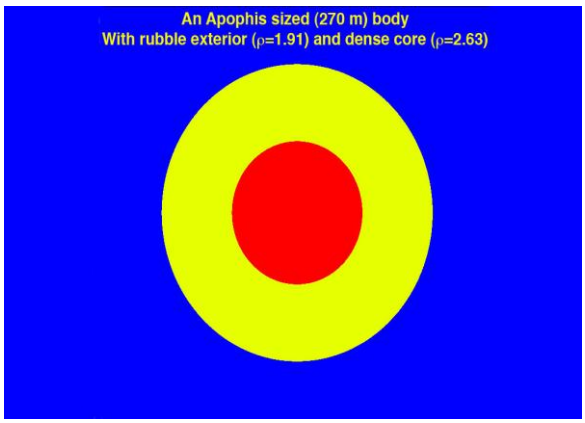

Fig. 1. An internal composition of a 270 m NEO [4]

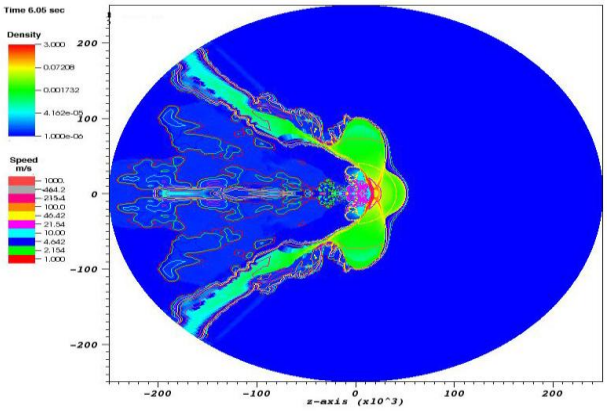

Fig. 2. Fragment Distribution of Static ALE Results [4]

where η is a material damage indicator, to be discussed later. It should be noted that fully damaged material ($\eta = 1$) is relieved of all stress due to deformation and behaves as a cohesionless fluid [8,10]. In this elastic-plastic model, the components of the deviatoric stress tensor $S^{\alpha\beta}$ evolve using the following equation based on Hooke's law [6,11]:

$$\frac{DS_i^{\alpha\beta}}{Dt} = 2\mu\left(\varepsilon_i^{\alpha\beta} - \frac{1}{3}\delta^{\alpha\beta}\varepsilon^{\gamma\gamma}\right) + S_i^{\alpha\gamma}R_i^{\beta\gamma} + R_i^{\alpha\gamma}S_i^{\gamma\beta} \tag{4}$$

where $R^{\alpha\beta}$ is the local rotation rate tensor, μ is the shear modulus, and the SPH approximation for these terms is:

$$\begin{aligned}
\varepsilon_i^{\alpha\beta} &= \frac{1}{2}\sum_{j=1}^{N}\frac{m_j}{\rho_j}\left[\left(v_j^{\alpha} - v_i^{\alpha}\right)\frac{\partial W}{\partial x^{\beta}}\left(\mathbf{x}_j - \mathbf{x}_i\right) + \left(v_j^{\beta} - v_i^{\beta}\right)\frac{\partial W}{\partial x^{\alpha}}\left(\mathbf{x}_j - \mathbf{x}_i\right)\right] \\
R_i^{\alpha\beta} &= \frac{1}{2}\sum_{j=1}^{N}\frac{m_j}{\rho_j}\left[\left(v_j^{\alpha} - v_i^{\alpha}\right)\frac{\partial W}{\partial x^{\beta}}\left(\mathbf{x}_j - \mathbf{x}_i\right) - \left(v_j^{\beta} - v_i^{\beta}\right)\frac{\partial W}{\partial x^{\alpha}}\left(\mathbf{x}_j - \mathbf{x}_i\right)\right]
\end{aligned} \tag{5}$$

To complete this system, we use the following equations governing the change of support radius h [6,7], and the fracture damage ratio η [8]. The latter is limited in accordance with the number of material flaws activated in the structure, as described in the next section:

$$\frac{Dh_i}{Dt} = -\frac{1}{n}\frac{h_i}{\rho_i}\frac{D\rho_i}{Dt}, \qquad \frac{D}{Dt}\eta^{1/3} = \frac{c_g}{r_s} \tag{6}$$

where c_g is the crack growth rate, here assumed to be 0.4 times the local sound speed [8], and r_s is the radius of the subvolume subject to tensile strain. In the present model, the latter term is estimated by interpolation based on the strain rate tensor of neighbor particles. An equation of state remains to complete the mechanical system. We use the Tillotson equation of state [12] in the solid asteroid core and in the Al penetrator used to deliver the explosive. This is modified to include porosity, and an irreversible crush strength, for the outer "rubble pile" layer [10,13].

Implicit Flaw Assignment

We assume a power law distribution for number of implicit flaws in a volume of material with respect to local tensile strain (a Weibull distribution), and assign flaws with specific activation thresholds to each SPH particle [8]. The maximum damage allowed to accumulate in a volume is:

$$\eta_i^{\max} = \left(\frac{n_i}{n_i^{tot}}\right)^{1/3}, \qquad \varepsilon_i = \frac{\sigma_i^t}{\left(1 - D_i\right)E} \tag{7}$$

where n_i is the number of active flaws ($\varepsilon > \varepsilon^{act}$) and n^{tot} is the total number of flaws assigned to a particle, which can vary widely, but is always at least one. Eq. (7) also gives the relationship for the local scalar strain, as a function of the maximum tensile stress σ^t, the local damage, and the Young's modulus E.

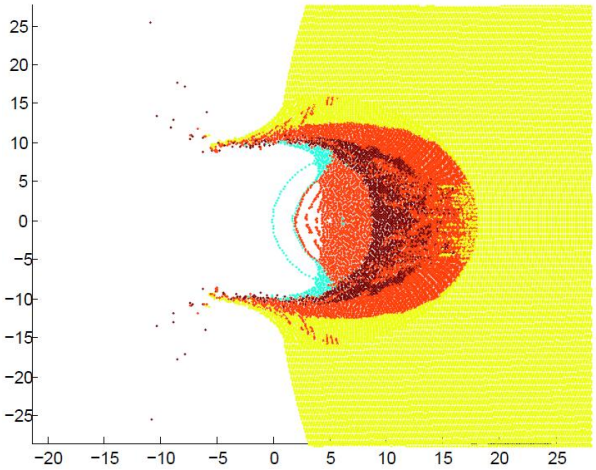

Fig. 3. 270 m Asteroid Penetrator at 2.3 ms

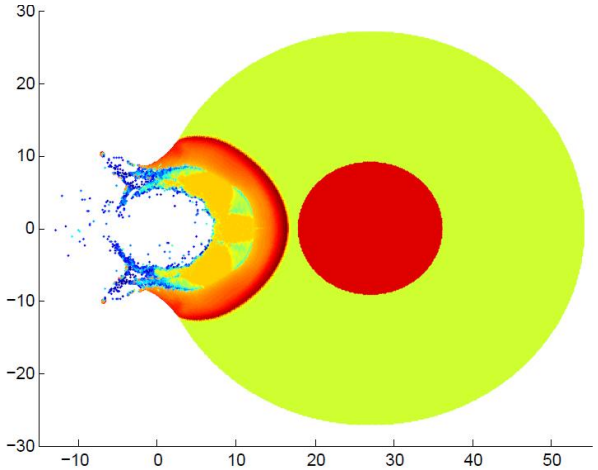

Fig. 4. Expanding Shock Wave Through Rubble at 2.3 ms

Resulting Fragmented System

The present models use a starting resolution of 0.1 m for two target asteroids with diameters of 270 m and 54 m, resulting in 1.4 million and 233,000 fragments, respectively. Penetrators impact the asteroids at a velocity of 6.1 km/s, and explode on contact, sourcing 300 kilotons and 60 kilotons into the model respectively. This can be seen in Fig. 3. The resulting hot gas of explosive remnants tunnels into the tuff material, crushing it to solid density before flashing much of it to liquid and dispersing the rubble and fracturing the core. An example of this increase in density for the 54 m target, with an expansion region behind the shock creating a jet of hot gas, can be seen in Fig. 4. The resulting mass-averaged fragment velocities are on the order of 10-100 m/s, similar to that for a static subsurface explosion [4], with a definite direction of highest momentum in the direction of the penetrator motion. An example distribution of these velocities is shown in Fig. 5. This simulation framework is equally valid for oblique impacts, and should allow for direct implementation in conjunction with deflection mission planning.

While the fragmentation model results in different results each time, we can average multiple runs to achieve a mean distribution that is representative of the physical situation. This simulation is not intended to be a prediction, but rather a way to determine general system behavior to identify particularly effective methods for disruption. The present SPH model is extremely fast, and is a good option for describing a fragmented asteroid system due to an explosive penetrator.

ORBITAL DISPERSION MODEL

This section describes the orbital model used to propagate fragment trajectories. The nominal orbit chosen is close to that of Apophis post-2029, with slight alterations made to ensure impact in our model on April 13, 2036. The parameters for this orbit are given in Table 1.

Table 1. Orbital Parameters for 15 day Impact Trajectory

Orbital Parameter	Value
Semimajor Axis	1.1082428 AU
Eccentricity	0.189928428
Inclination	2.18995362 deg
Longitude of Right Ascension	203.18642266 deg
Argument of Perihelion	69.929774 deg
Initial Mean Anomaly	296.74684241 deg
Epoch	64781 MJD
Miss Distance on Target Date	4.738466849E-011 Earth Radii

Equations of Motion

The debris cloud is given global coordinates in a Local-Vertical-Local-Horizontal (LVLH) reference frame about the center of mass, as shown in Fig. 6. These are then integrated to predict an ephemeris for a 48 hour period surrounding the nominal time of impact. Since coherent clouds of asteroid debris can reaggregate into a rubble pile for subcritical disruption energies [1,14,15], or remain a field of disruptive bodies [15,16], we implement a system for computing self-gravity among the resulting fragments. Since the LVLH reference frame is computationally beneficial for self-gravity

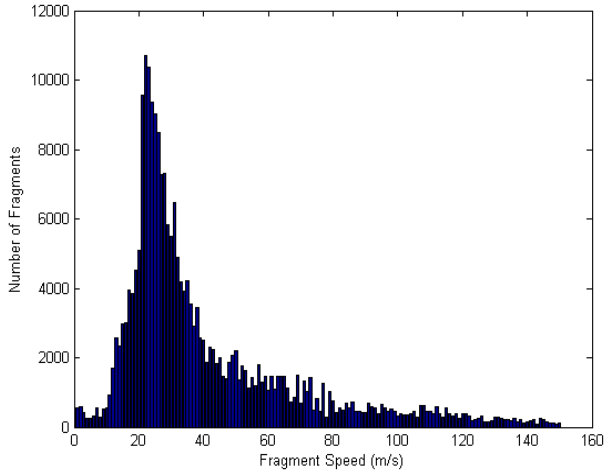

Fig. 5. Example Fragment Velocity Distribution

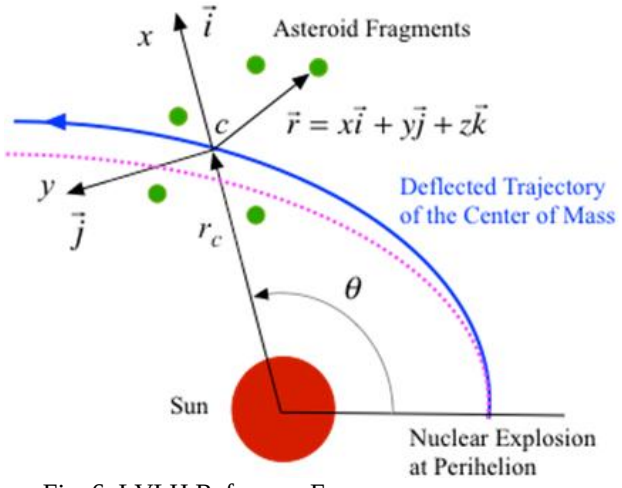

Fig. 6. LVLH Reference Frame

and collision modelling among fragments [1], we use the nonlinear relative equations of motion for this frame to govern fragment trajectories [1,5]:

$$\begin{aligned}
\ddot{x}_i &= 2\dot{\theta}\left(\dot{y}_i - \frac{\dot{r}_c}{r_c}y_i\right) + \dot{\theta}^2 x_i + \frac{\mu}{r_c^2} - \frac{\mu}{r_d^3}\left(r_c + x_i\right) + \frac{\mu_E}{r_{Ei}^3}\left(x_E - x_i\right) + F_i^x \\
\ddot{y}_i &= -2\dot{\theta}\left(\dot{x}_i + \frac{\dot{r}_c}{r_c}x_i\right) + \dot{\theta}^2 y_i - \frac{\mu}{r_d^3} + \frac{\mu_E}{r_{Ei}^3}\left(y_E - y_i\right) + F_i^y \\
\ddot{z}_i &= -\frac{\mu}{r_d^3}z_i + \frac{\mu_E}{r_{Ei}^3}\left(z_E - z_i\right) + F_i^z
\end{aligned} \tag{8}$$

where x, y, z, r_c, and θ are defined as shown in Fig. 6, r_d is the length of the relative coordinate vector, μ and μ_E are gravitational parameters for the sun and the Earth, r_{Ei} is the distance from each fragment to Earth, and (F^x, F^y, F^z) are the combined acceleration components due to 3rd body gravitational terms (solar system major body model [5]), self-gravity, and collision corrections. The threading structure for computing the values for self gravity terms is described in [1], while collisions are predicted using a Sort-and-Search algorithm [17], resulting in post-collision changes to position and velocity of fragments. An elastic spherical collision model is assumed for the fragments, with a coefficient of restitution of 0.5.

The mass left on impacting trajectories is around 0.1% for a radial (outward) deflection with 15 days between the deflection attempt and the impact date. This target window is extremely beneficial from an engineering standpoint, as there is strong coupling between time-to-impact and a reduction in mission fuel cost [18]. High energy methods such as nuclear explosives are the only known way to produce results on such a short time frame. The present work shows that a well-designed impactor mission can achieve similar results with a contact burst as were previously predicted for a subsurface explosion. The benefit to the former method is that is does not require a rendezvous, and therefore there are available launch windows for this orbit over the entire period from 2029-2036 [18].

Reentry Model

For the fragments remaining on trajectories impacting Earth, we simulate reentry assuming solid granite material (a worst case) and a static (time independent) atmospheric density [5]. This gives a rough estimate on the amount of material ablated through atmospheric heating and the number of fragments that are deflected or disrupted by the atmosphere. This has been shown to reduce the amount of impacting mass by about 90% [5]. While the remaining fragments could cause significant harm in populated areas, or through tsunami events, the impacts are below the threshold for an extinction event. This may indicate that nuclear disruption would be a desired outcome for a late-notice or late-decision scenario. Geocentric coordinates of these impacting events are calculated in order to provide a description of distance between impacts in both space and time. An example of this is shown in Fig. 7.

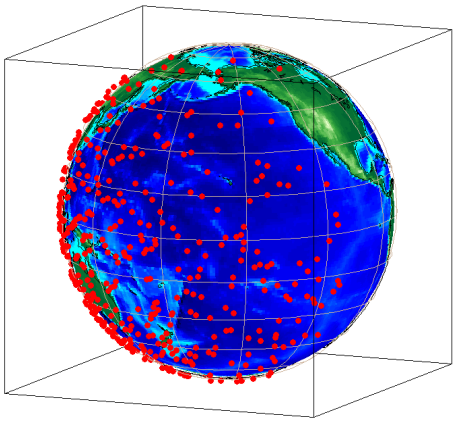

Fig. 7. Example Impact Location Distribution [5]

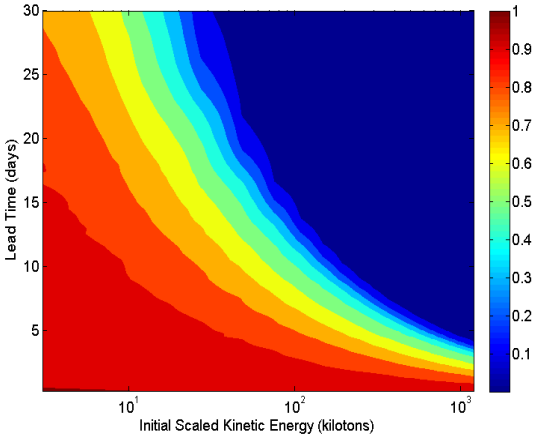

Fig. 8. Contour Plot for Impact Mass Parameter Study [2]

Timing and Initial Explosive Energy

Fast computation of the resulting fragmented system allows for rapid parameter variation to determine optimal mission design parameters. Two quantities of significant interest are the amount of lead time between deflection and impact, and the amount of kinetic energy imparted to the fragments in the deflection event. One result of this study is the understanding that conventional explosives do not provide enough energy to deflect the majority of a 270 m asteroid with up to 1 full orbit lead time (~1000 days) [2]. An example of how impacting mass changes with timing and initial energy scaling can be seen in Fig. 8. Additionally, the benefit of additional lead time slows substantially above 30 days, revealing that 30 days might be a good target for mission design. For lead times below 10 days, an adequate deflection measure requires far more energy than generally available, suggesting the need for multiple deflection missions in this regime [2].

COMPUTATIONAL STRUCTURE

This section address the computational approach used to solve the disruption problem. Each state variable update for a fragment is conducted in parallel at each time step. A variety of hardware was available for this project, with a substantial difference in performance. This allowed us to get reasonable estimates on the computational cost of this simulation, in comparison to LINPACK performance numbers. Performance can vary based on the type of arrays used, and the number of threads dedicated to each GPU calculation. These factors are determined by the CUDA Compute Capability (CUDA CC), which is a property of the GPU [3]. These cost estimates are used to determine hardware performance on the various systems. A summary of the hardware used is shown in Table 2 (Note: all CPUs are Intel brand, and all GPUs are NVIDIA brand).

Table 2. Hardware for Benchmark Systems

System	Machine 1	Machine 2	Machine 3	Machine 4	Machine 5
CPU	1x Core2 Q6600	1x Core2 Q6600	1x Xeon X5550	2x Xeon E5520	2x Xeon X5650
CPU Cores	4	4	4	8	12
CPU TPEAK	9.6 GFLOPs	9.6 GFLOPs	12.8 GFLOPs	21.36 GFLOPs	32.04 GFLOPs
GPU	1x 8800GTS	1x GTX470	1x GTX480	4x Tesla c1060	4x Tesla c2050
GPU Cores	112	448	480	960	1792
GPU TPEAK	84 GFLOPs	324 GFLOPs	385 GFLOPs	336 GFLOPs	2060 GFLOPs
CUDA CC	CC 1.0	CC 2.0	CC 2.0	CC 1.3	CC 2.0

Each thread on the GPU calculates the state variable change for one fragment, with the GPU kernel limited to one time step. This is necessary because the positions of the planets and other gravitating bodies must be calculated and transferred to the GPU at each time step. Additionally, the positions of fragments at each integration substep are shared among multiple GPUs and CPU threads. For this reason, the present model is predominantly bandwidth-limited for small data sets. While grid information is not retained, one of the disadvantages of the SPH hydrocode is that neighboring particles must be calculated at each time step. Our approach in this model is to create a bounding volume for each SPH particle and perform the same Sort and Sweep in parallel as used to detect collisions in the orbital model [17]. We retain the information for neighbors connected by material strength, as well as carrying neighbor information through the correction step of the integrator. This results in a 28% performance improvement over recalculating neighbors at both the prediction and correction steps, while allowing for a variable time step based on the Courant condition [6,7]:

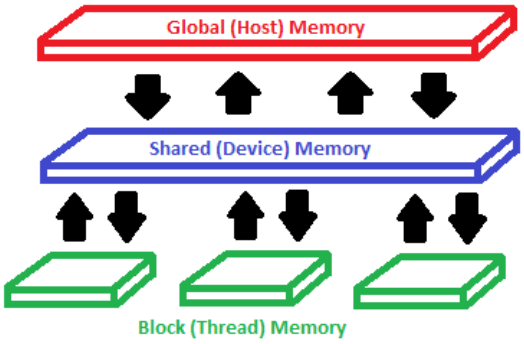

Fig. 9. Qualitative Computational Memory Model

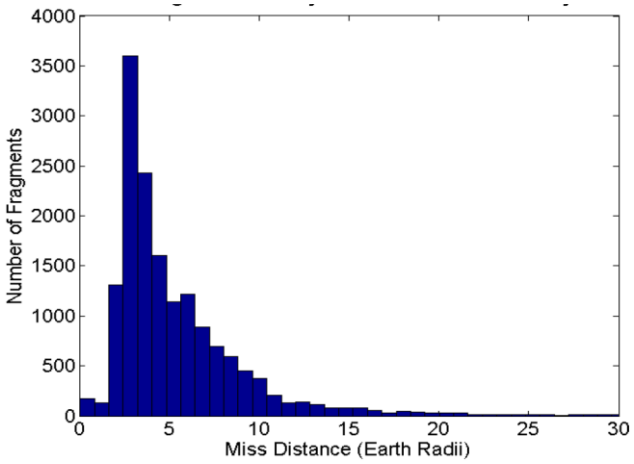

Fig. 10. Miss Distance Histogram for 15 Day Lead Time

$$\delta t = \min_i \frac{h_i}{c_i} \tag{9}$$

where c is the local sound speed. While the reduction operation to determine the new time step can be done in parallel, all GPU threads must have position information for all particles to determine neighbors. This requirement could be eliminated through clever domain decomposition, but there is a tradeoff between associating a mesh to the model and taking advantage of contiguous memory sections of particles. Load balancing would also require additional communication between GPUs, which has an impact on performance, as PCI-E bandwidth is one of the limiting factors in GPU acceleration [3].

Our memory model for this simulation includes a shared host memory, distributed device memory for each GPU, and data transfers between them handled through explicit array transfer. Each block of compute threads on the GPU takes the data it needs from the global device memory when the kernel reaches its block. This is an important factor, because the varying compute capabilities have different limitations on this block memory, changing the number of threads that may be used in the calculation. Constants are transferred to all GPU memories implicitly using a pointer to the host constant value. Fig. 9 shows an overview of this computational memory model.

While modern dedicated compute GPUs have a high amount of onboard memory, it usually is far less than system memory. Though it may seem advantageous to calculate parameters for every time step before the start of the simulation, the arrays resulting from this approach are quite large. Each model of GPU has a limited number of memory registers available to each computing block of threads [3]. Therefore, the use of several large arrays can actually slow down the simulation in some cases, by lowering the number of threads below the maximum allowed by the architecture. This trades off directly with the added expense of calculating parameters on the Host at each time step. For the present work, calculating planetary positions and other simulation parameters at each step was found to be preferable to using a large pre-calculated array. For some hardware, sufficient GPU memory was not available for the latter method, so a heterogeneous computing approach proved to be the most portable.

CONCLUSIONS

As shown in Fig. 10, the impacting mass for a fragmented system with 15 day lead time can be very low, even including self-gravity and collisions among the fragments that dissipate energy. The present SPH hydrocode suggests that a dynamic model of a hypervelocity surface burst yields results similar in spatial and temporal distribution to a static subsurface explosion. This gives additional launch windows for mission design, limits the fuel needed for a rendezvous burn, and avoids the need to bury the explosive payload. Additionally, the dynamic model should better predict system behavior when addressing high velocity penetrator architectures. This might give an option for realistically determining the limits of such a system for asteroid deflection missions.

New HPC technology utilizing GPU acceleration have resulted in orders of magnitude improvement in computational ability. Figs. 11 and 12 show speedup of the GPU accelerated model compared to serial execution for the 54 m and 270 m target models. While the 233,000 particles of the 54 m target are limited mostly by communication bandwidth, the 1.4 million particles in the 270 m model are limited by computational speed and memory bandwidth for the threads on the GPU. A substantial speedup improvement, from 454x to 632x, is observed. This shows single node computational performance on the same order as a moderate cluster. The ability to run multiple cases to address statistical system behavior results in simulation being integrated into overall mission design. Mission effectiveness can be estimated in

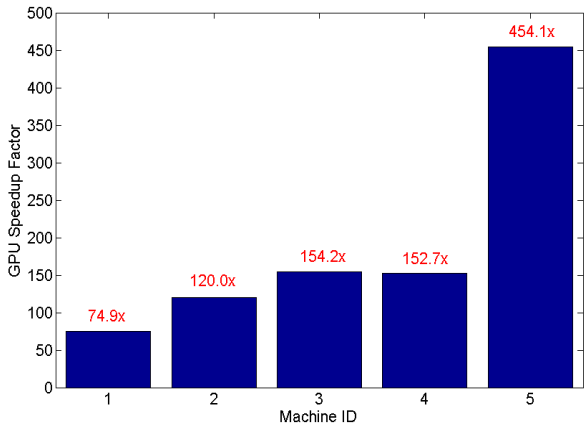

Fig. 11. GPU Speedups for 54 m Target Asteroid Model

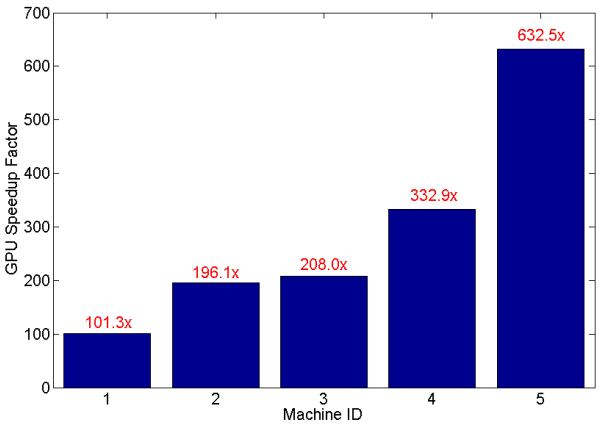

Fig. 12. GPU Speedups for 270 m Target Asteroid Model

advance of a need for mission design, allowing new architectures and interchangeable components for a universal deflection plan.

This paper outlined the development of software and hardware tools to aid the planning of NEO deflection mission design, and the current project strives to identify key technologies for effective implementation. We now have the technology and resources to move from threat to action, and a new era of planetary defense where we can focus on developing a standing threat mitigation capability is on the horizon.

REFERENCES

[1] B. Kaplinger and B. Wie, "Optimized GPU Simulation of a Disrupted Near-Earth Object Including Self-Gravity," AAS-11-266, *21st AAS/AIAA Spaceflight Mechanics Meeting*, New Orleans, LA, February 13-17, 2011.

[2] B. Kaplinger and B. Wie, "Parameter Variation In Near-Earth Object Disruption Simulations Using GPU Acceleration," AAS-11-267, *21st AAS/AIAA Spaceflight Mechanics Meeting*, New Orleans, LA, Feb. 13-17, 2011.

[3] D.B. Kirk and W.W. Hwu, *Programming Massively Parallel Processors*, Burlington: Morgan Kaufmann, 2010.

[4] B. Wie and D. Dearborn, "Earth Impact Modeling and Analysis of a Near-Earth Object Fragmented and Dispersed by Nuclear Subsurface Explosions," AAS-10-137, *20th AAS/AIAA Spaceflight Mechanics Meeting*, San Diego, CA, February 14-17, 2010.

[5] B. Kaplinger, B. Wie, and D. Dearborn, "Preliminary Results for High-Fidelity Modeling and Simulation of Orbital Dispersion of Asteroids Disrupted by Nuclear Explosives," AIAA-2010-7982, *AIAA/AAS Astrodynamics Specialist Conference*, Toronto, Ontario, Canada, August 2-5, 2010.

[6] J.J. Monaghan, "Smoothed Particle Hydrodynamics," *Rep. on Prog. in Physics*, vol. 68, pp. 1703-1759, July 2005.

[7] G.R. Liu and M.B. Liu, *Smoothed Particle Hydrodynamics: A Meshfree Particle Method*, Singapore: World Scientific Publishing, 2003.

[8] W. Benz and E. Asphaug. "Simulations of Brittle Solids using Smooth Particle Hydrodynamics," *Computer Physics Communications*, vol. 87, pp. 253-265, 1995.

[9] S. Hiermaier, D. Konke, A.J. Stilp, and K. Thoma, "Computational Simulation of the Hypervelocity Impact of Al-Spheres on Thin Plates of Different Materials," *Intl. Journal of Impact Engineering*, vol. 20, pp. 363-374, 1997.

[10] M. Jutzi, W. Benz, and P. Michel, "Numerical Simulations of Impacts Involving Porous Bodies I. Implementing Sub-Resolution Porosity in a 3D SPH Hydrocode," *Icarus*, vol. 198, pp. 242-255, 2008.

[11] P.W. Randles and L.D.Libersky, "Smoothed Particle Hydrodynamics: Some Recent Improvements and Applications," *Computer Methods in Applied Mechanics and Engineering*, vol. 139, pp. 375-408, 1996.

[12] J.H. Tillotson, "Metallic Equations of State for Hypervelocity Impact," General Atomic Technical Report GA-3216, 1962.

[13] S.H. Schuster and J. Isenberg, "Equations of State for Geologic Materials," Defense Nuclear Agency Technical Report DNA-2925Z, 1972.

[14] S.G. Love and T.J. Ahrens, "Catastrophic Impacts on Gravity Dominated Asteroids," *Icarus*, vol. 124, pp. 141-155, 1996.

[15] E. Asphaug, S.J. Ostro, R.S. Hudson, D.J. Scheeres, and W. Benz, "Disruption of Kilometre Sized Asteroids by Energetic Collisions," *Nature*, vol. 393, pp. 437-440, 1998.

[16] P. Michel, W. Benz, and D.C. Richardson. "Disruption of Fragmented Parent Bodies as the Origin of Asteroid Families," *Nature*, vol. 421, pp. 608-611, February 2003.

[17] S. LeGrand, "Broad-Phase Collision Detection with CUDA," *GPU Gems 3*, ed. H. Nguyen, Addison-Wesley, 2007.

[18] S. Wagner and B. Wie, "Analysis and Design of Fictive Post-2029 Apophis Intercept Mission for Nuclear Disruption," AIAA-2010-8375, *AIAA/AAS Astrodynamics Specialist Conference*, Toronto, Ontario, Canada, August 2-5, 2010.